DOI: https://doi.org/10.24425/amm.2026.157782

HAITAO MA[1,2*], YANHUI SUN[2]

NUMERICAL SIMULATION OF CRACK SENSITIVITY IN HEAVY RAIL STEEL BLOOMS UNDER REDUCTION CONDITIONS

In this study, a numerical simulation approach was employed to evaluate the risk of crack initiation during the reduction process of a 230 mm × 280 mm section bloom of heavy rail steel. The simulation results indicated that no internal cracking was expected when the per-pass reduction was set to 1 mm and 3 mm. When the single-pass reduction was increased to 5 mm and the central solid fraction of the 230 mm × 280 mm section bloom of heavy rail steel fell below 0.40, the risk of internal crack formation increased significantly. Concurrently, an industrial-scale validation test was conducted, revealing that the crack-sensitive zone of the 230 mm × 280 mm section bloom of heavy rail steel was primarily associated with regions where the central solid fraction was below 0.42. The findings indicated that decreasing the reduction amount or shifting the reduction zone downstream could effectively reduce the risk of crack formation in heavy rail steel blooms. The experimental results confirmed the reliability of the proposed mathematical model.

Keyword: Heavy rail steel; Reduction technology; Crack sensitivity; Numerical simulation

Introduction

Heavy rail steel is a high-carbon specialty steel that is prone to developing internal quality defects, such as porosity, shrinkage cavities, and centerline segregation, during the continuous casting process [1-4]. Among the various approaches to enhance the internal quality of blooms, final solidification-stage reduction has been recognised as one of the most effective methods and is widely implemented across the iron and steel industry [5-7]. However, in actual production, the improper selection of reduction parameters can readily lead to the formation of internal cracks in the bloom [8-12]. This issue has been the subject of extensive investigation by numerous researchers. Song [13] performed a thermos-mechanical coupling numerical simulation for a 280 mm × 380 mm large square bloom of heavy rail steel and found that internal cracks did not occur when the reduction amount was less than 3 mm. However, when the reduction amount reached 5 mm, the solid fraction did not exceed 0.40. Wang [14] investigated the formation mechanism of internal cracks induced by bloom reduction and concluded that tensile strain-induced tearing was the primary cause of crack initiation under such conditions. Li [15] reported that internal cracks predominantly formed between the zero strength temperature (ZST) and the zero ductility temperature (ZDT). Similarly, Yamanaka [16] and Kobayashi [17] determined that the central solid fraction of the bloom within the ZST-ZDT range was between 0.80 and 0.99.

Based on the production conditions of heavy rail steel blooms in an industrial facility, a mathematical model for reduction was developed using ABAQUS finite element software. The effects of various process parameters on the stress and strain distribution within the bloom were analyzed, and the risk of internal crack formation was predicted. This approach enabled the optimization of continuous casting parameters, thereby enhancing bloom quality.

1. Development of the mathematical model

1.1. Model assumption

A thermos-mechanical coupling mathematical model was developed to predict the risk of internal crack formation in a 230 mm × 280 mm section bloom of heavy rail steel. To ensure

[1] MCC CAPITAL ENGINEERING & RESEARCH INCORPORATION LIMITED, STEEL MAKING DEPARTMENT, BEIJING 100176, CHINA
[2] UNIVERSITY OF SCIENCE AND TECHNOLOGY BEIJING, COLLABORATIVE INNOVATION CENTER OF STEEL TECHNOLOGY, BEIJING, 100083, CHINA
* Corresponding author: mahaitao240004@ceri.com.cn

© 2026. The Author(s). This is an open-access article distributed under the terms of the Creative Commons Attribution License (CC-BY 4.0). The Journal license is: https://creativecommons.org/licenses/by/4.0/deed.en. This license allows others to distribute, remix, modify, and build upon the author's work, even commercially, as long as the original work is attributed to the author.

the accuracy of the calculation results, the following assumptions were adopted.

(1) Heat transfer in the casting direction of the bloom was neglected.
(2) The temperature along the casting direction of the bloom was assumed to be uniform, the solidified shell thickness was considered constant, and the influence of liquid steel pressure on the solidified shell was not neglected.
(3) The material was assumed to conform to the small deformation theory, and deformation in the force direction of the bloom was neglected.
(4) The material was assumed to be homogeneous, and the influence of its microstructure was neglected.

1.2. Governing equation

It was assumed that heat transfer in the casting direction of the bloom was negligible, and the solidification process was treated as a two-dimensional transient heat transfer problem with an internal heat source.

The governing equation is expressed as follows (Eq. 1):

$$\rho c \frac{\partial T}{\partial t} = \frac{\partial}{\partial x}\left(\lambda \frac{\partial T}{\partial x}\right) + \frac{\partial}{\partial y}\left(\lambda \frac{\partial T}{\partial y}\right) + Q \tag{1}$$

Where ρ is the density ($kg \cdot m^{-3}$), c is the specific heat ($J \cdot kg^{-1} \cdot °C^{-1}$), T is the temperature (°C), t is the time (s), λ is the effective thermal conductivity ($W \cdot m^{-1} \cdot K^{-1}$), and Q represents the internal heat source ($W \cdot m^{-3}$). Based on the heat transfer model of the bloom, the temperature field in the reduction region was calculated. The resulting temperature field data were then extracted and applied as the initial temperature conditions in the thermos-mechanical coupling mode.

During the reduction process, the bloom was subjected to roller pressure, resulting in both elastic and plastic deformation. At elevated temperatures, thermal strain was also generated. During the solidification process, the stress-strain relationship was assumed to be in a steady state. Based on the elastic-plastic incremental theory, the total strain of the bloom is expressed as follows (Eq. 2):

$$\{d_\varepsilon\} = \{d\varepsilon_e\} + \{d\varepsilon_p\} + \{d\varepsilon_T\} \tag{2}$$

Where $\{d_\varepsilon\}$ is the total strain increment, $\{d\varepsilon_e\}$ is the elastic strain increment, $\{d\varepsilon_p\}$ is the plastic strain increment, and $\{d\varepsilon_T\}$ is the thermal strain increment.

(1) Elastic strain increment

According to Hooke's law, the elastic strain increment in the elastic deformation stage is expressed as follows (Eq. 3):

$$\{d\varepsilon_e\} = [D_e]^2 \{d\sigma\} \tag{3}$$

Where $[D_e]$ is the elastic matrix.

(2) Plastic strain increment

In the plastic deformation stage, the plastic strain is expressed as follows (Eq. 4):

$$\{d\varepsilon_p\} = d\lambda \frac{\partial \varphi}{\partial \sigma} \tag{4}$$

Where λ is the constant, φ is the Mises yield function, and σ is the stress (Pa).

During the process of plastic deformation, the relationship between stress and strain is as follows (Eq. (5)-(8)):

$$\varepsilon_p = C \exp\left(\frac{-Q}{T}\right) \sigma^n t^m \tag{5}$$

$$C = 0.3091 + 0.2090 w_{[c]} + 0.1773 w_{[c]}^2 \tag{6}$$

$$n = 6.365 - 4.521 \times 10^{-3} T + 1.439 \times 10^{-6} T^2 \tag{7}$$

$$m = -1.362 + 5.761 \times 10^{-4} T + 1.982 \times 10^{-8} T^2 \tag{8}$$

Where C, m, n is coefficient; $w_{[c]}$ is carbon content (%); Q is deformation activation energy; T is the temperature, (°C); σ is the stress(Pa); t is the time, (s).

(3) Thermal strain increment

The thermal strain increment is expressed as follows (Eq. 9):

$$\{d\varepsilon_T\} = \{\alpha\} dT \tag{9}$$

Where $\{\alpha\}$ is the thermal expansion coefficient matrix.

1.3. Initial conditions and boundary conditions

(1) Initial conditions

The temperature of the molten steel in the mold is equal to the pouring temperature (Eq. 10):

$$T(x, y, 0) = T_c \tag{10}$$

Where, T_c is the casting temperature, (°C);

The temperature field data obtained from the solidification heat transfer model at the reduction stage were extracted and used as the initial condition for the thermal strain model. The stresses generated during the solidification process of the bloom were neglected. The bloom was assumed to be in instantaneous contact with the upper and lower rollers during reduction, without the application of any external force.

(2) Boundary conditions

The Boundary Condition was set as follows:

During the solidification process of the bloom, it mainly goes through the cooling in the mold, the secondary cooling zone and the air cooling radiation zone. The heat transfer mechanism on the surface of the bloom varies in each of these three cooling zones.

Heat transfer in the mold (Eq. (11)-(13)):

$$q_m = 2680000 - b\sqrt{L/v} \tag{11}$$

$$b = 1.5 \times \left(2680000 - \bar{q}\right)\sqrt{L_m / v} \tag{12}$$

$$\bar{q} = \frac{\rho_w c_w Q_w \Delta T_w}{S_{eff}} \tag{13}$$

Where, q_m is the heat flux density of the bloom surface the mold, ($kW \cdot m^{-2}$); v is the casting speed, ($m \cdot min^{-1}$); L is the distance from the location of the heat flow to meniscus, m; L_m is the effective length of the mold, (m); $\bar{q}$ is the average heat flux density of the mold, ($kW \cdot m^{-2}$); ρ_w is the density of cooling water, ($kg \cdot m^{-3}$); c_w is the specific heat of cooling water, ($J \cdot kg^{-1} \cdot °C^{-1}$); Q_w is Cooling water flow rate of the mold, ($m^3 \cdot s^{-1}$); ΔT is the water temperature difference, (°C); S_{eff} is the effective contact area between the molten steel and the copper plate of the mold, (m^2).

Heat transfer in the secondary cooling zone (Eq. (14)-(15)):

$$q_s = h(T_b - T_0) \tag{14}$$

$$h = 0.151 \cdot W^{0.55} \tag{15}$$

Where, q_s is the heat flux density of the bloom surface in the secondary cooling zone, ($W \cdot m^{-2}$); h is the convective heat transfer coefficient, ($W \cdot m^{-2} \cdot K^{-1}$); T_b is the surface temperature of the bloom, (°C); T_0 is the environmental temperature, (°C); W is the water flow density, ($L \cdot m^{-2} \cdot s^{-1}$).

Heat transfer in air-cooling zone (Eq. 16):

$$q_s = \varepsilon\sigma\left[\left(T_b + 273.15\right)^4 - \left(T_0 + 273.15\right)^4\right] \tag{16}$$

Where, ε is the radiation coefficient, 0.8; σ is the Boltzmann constant, 5.67×10^{-8}; T_b is the surface temperature of the bloom, (°C); T_0 is the environmental temperature, (°C);

Thermal analysis boundary conditions: The reduction section was treated as an air cooling zone, and radiative heat transfer from the bloom surface was considered. The two ends of the bloom cross-section were assumed to be in an adiabatic state.

Structural analysis boundary conditions: The bloom was assumed to remain stationary, while the upper and lower rollers applied compression corresponding to the reverse displacement of the casting speed. The surface of the bloom was treated as a free surface. For the two cross sections at the front and rear of the bloom, the bitten cross section was modeled as a free plane, while the unbitten cross section was constrained to have zero displacement in the casting direction.

1.4. Mathematical model

The reduction geometry model for the 230 mm × 280 mm section bloom of heavy rail steel comprised three components: the bloom, the reduction roll, and the supporting roll. The rolls had a radius of 0.21 m and a width of 0.29 m. The 0.5 m length of the bloom was selected as the study domain. The geometric model is shown in Fig. 1, where NT11 denotes the node temperature.

Since the yield strength of the bloom was significantly lower than that of the lower roll and supporting roll, the bloom was modeled as an elastic material, while the reduction and supporting rolls were treated as rigid bodies. In the thermal strain model, C3D8T elements were employed. A transient temperature-displacement coupling analysis was employed in the model. The casting speed was set to 0.95 m/min, the casting temperature was 1495°C.While the initial temperatures of both the reduction roll and supporting roll were 200°C. The rotational speed of the rolls was 0.075 rad/s.

The heavy rail steel bloom was selected as the research object, and its chemical composition is presented in TABLE 1. The calculated solidus and liquidus temperatures of the heavy rail steel were 1365°C and 1470°C, respectively. The solidus and liquidus temperatures were used to identify the crack-sensitive zone within the temperature field. The relevant physical parameters of the mold cooling water, as well as the lengths and water flow rate of the secondary cooling zones, are shown in TABLES 2 and 3. Physical property parameters, including thermal conductivity, density, specific heat capacity, thermal expansion coefficient, elastic modulus, and Poisson's ratio, as well as the flow stress curve, were calculated and are presented in Figs. 2 and 3.

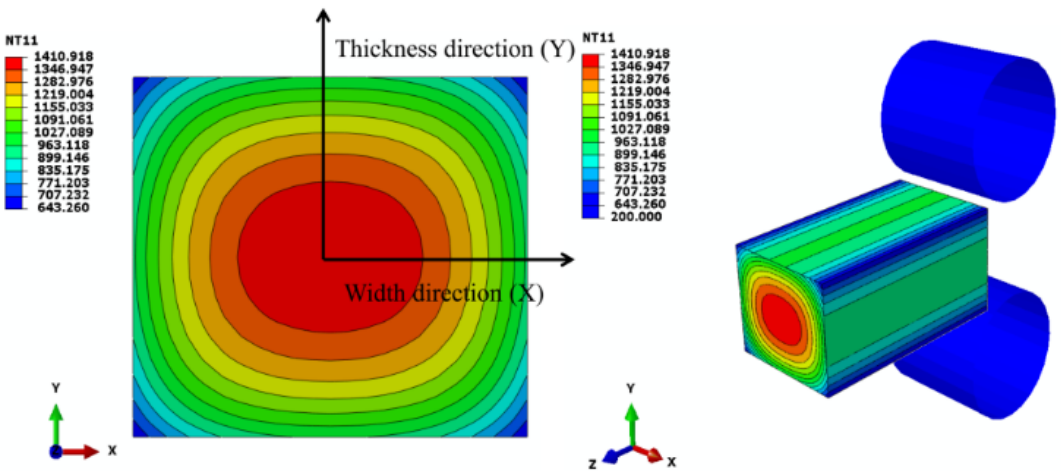

Fig. 1. The reduction model diagram of the bloom

TABLE 1

Chemical composition of heavy rail steel

Steel grade	C	Si	Mn	P	S	Cr
U71Mn	0.70	0.25	1.15	0.005	0.008	0.08

TABLE 2

The lengths and water flow rates of the second cooling zone

	Mold	Foot Zone	II Zone	III Zone	IV Zone
Length (m)	0.8	0.39	2.0	2.0	2.4
Water flow rate (L/min)	2500	46	51	30	21

TABLE 3

Parameters related to the cooling water of the mold

	Specific heat of cooling water ($J \cdot kg^{-1} \cdot °C^{-1}$)	Density of cooling water ($kg \cdot m^{-3}$)	ΔT (°C)
Value	4200	1000	7

2. Calculation of critical strain of heavy rail steel

Determining the stress and strain levels at the solidification front that can initiate cracks is a critical issue. However, most researchers have concluded that the strain at the solidification front is a more appropriate criterion for assessing the likelihood of internal crack formation [18-21]. Hiebler [22] compiled extensive research data and established the relationship between critical strain and the carbon equivalent of steel composition, as illustrated in Fig. 4.

By calculating the carbon equivalent and the [Mn]/[S] ratio of the steel, the critical strain for crack initiation can be determined. According to Eq. (17) and based on the chemical composition of the heavy rail steel, the carbon equivalent was 0.69%, and the [Mn]/[S] ratio was 143.8. As shown in Fig. 4, the corresponding critical strain for the heavy rail steel was 0.40%.

$$C_{eq} = [\%C] + 0.02[\%Mn] + 0.04[\%Ni] - 0.1[\%Si] - 0.04[\%Cr] - 0.1[\%Mo] \quad (17)$$

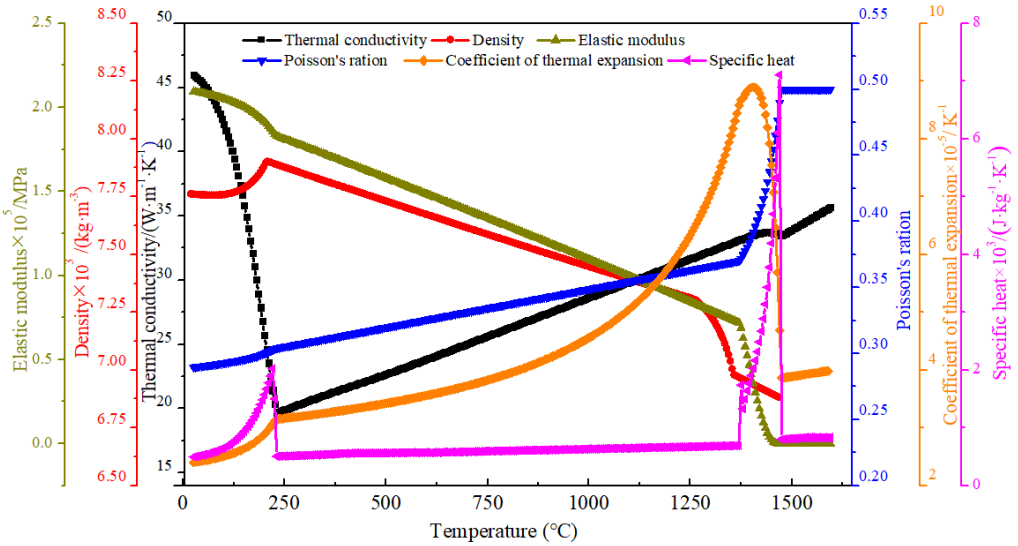

Fig. 2. Physical parameters of the heavy rail steel grade

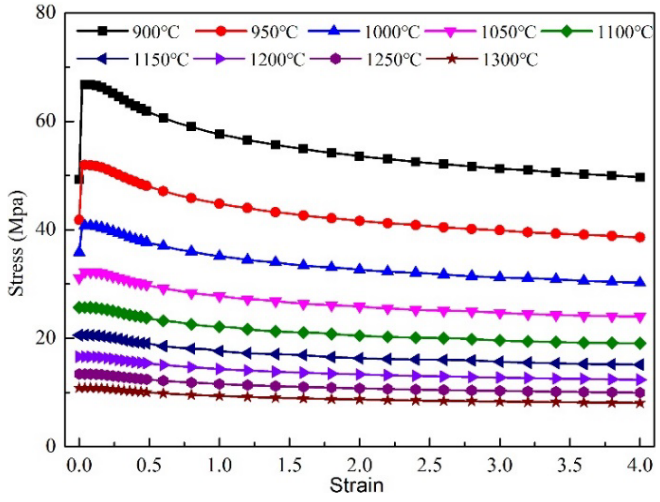

Fig. 3. Stress-strain curve of the heavy rail steel grade

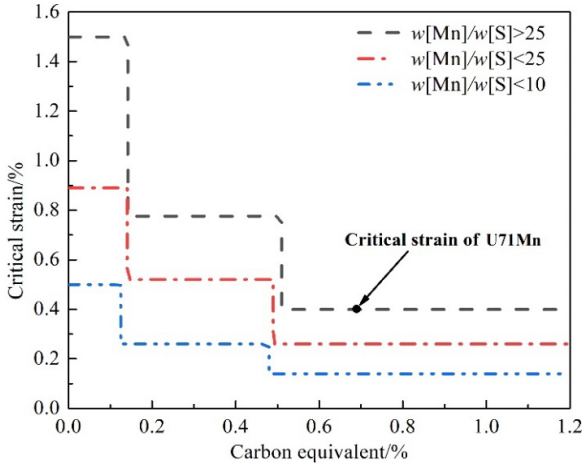

Fig. 4. The relationship between carbon equivalent and critical strain of steel composition

3. Discussion and analysis of the results

3.1. Temperature distribution of bloom cross section at different positions

Fig. 5 illustrates the distribution of the center temperature, surface temperature and solid fraction at the bloom of a 230 mm × 280 mm section of heavy rail steel bloom. The results indicate that, at the mould exit, the bloom surface exhibits a distinct reheating phenomenon. Once the bloom core was fully solidified, the center temperature dropped markedly as the release of latent heat was completed. At a casting speed of 0.95 m/min, the solidification end point was positioned 18.8 m from the meniscus, located between the 3# and 4# rollers. Based on the central solid fraction of the heavy rail steel bloom, rollers 0#, 1#, 2# and 3# were positioned within the mushy zone. The corresponding central solid fractions at these locations were 0.25, 0.40, 0.53, and 0.75, respectively. Therefore, at a casting speed of 0.95 m/min, the risk of internal crack formation induced by a reduction in the 230 mm × 280 mm heavy rail steel bloom was predicted to occur within the central solid fraction range of 0.25~0.75.

Fig. 6 presents the cross-sectional temperature distribution of the heavy rail steel bloom at various positions, where NT11 denotes the node temperature. As illustrated, with an increase in the central solid fraction, the bloom's core temperature progressively decreased, accompanied by a corresponding reduction in the liquid-phase thickness. The solidification front can be classified into a crack brittle zone and a crack sensitive zone, with the crack brittle zone defined as the region between the ZST and ZDT. According to previous research, the crack-sensitive zone lies between the LIT and ZDT. The corresponding solid fractions at the ZST, the LIT, and the ZDT were 0.75, 0.884, and 1.00, respectively. Based on JMatPro software calculations, the ZST, LIT, and ZDT of the heavy rail steel were determined to be 1391°C, 1377°C, and 1365°C, respectively.

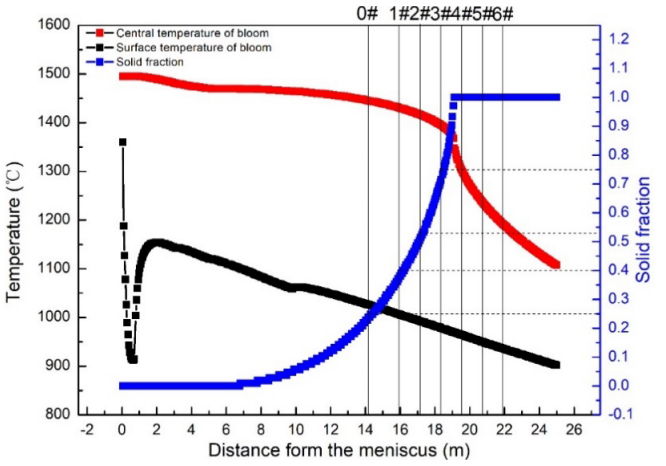

Fig. 5. Central temperature, surface temperature and central solid fraction of the bloom

Fig. 7 presents the temperature distribution along the thickness direction of the heavy rail steel bloom at various positions. As shown, the distance between the ZST and the ZDT in the cross section corresponded to 53.2-60.1 mm, 48.5-5.3 mm, 39.4-47.8 mm, and 27.5-39.0 mm at central solid fractions of 0.25, 0.40, 0.53, and 0.75, respectively. The brittle zone of the solidification front in the bloom cross-section at different positions was determined. The distances between the LIT and the ZDT from the bloom center measured 56.2-60.1 mm, 52.5-55.3 mm, 43.8-47.8 mm, and 33.9-39.0 mm, respectively. Accordingly, the crack-sensitive regions of the solidification front across the bloom cross-section at these positions were identified.

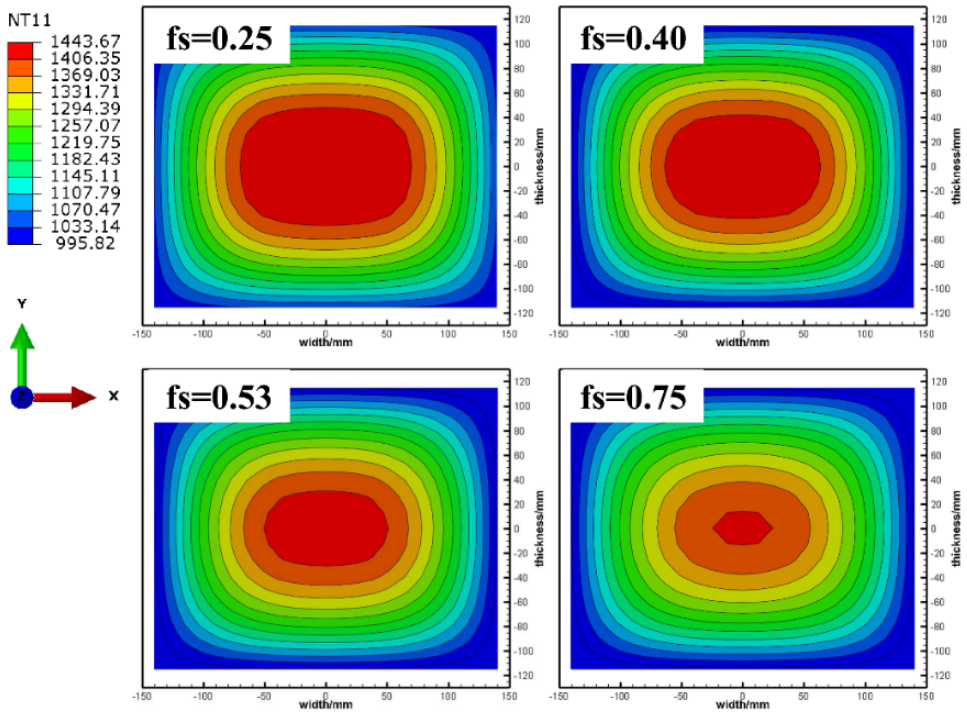

Fig. 6. The cross-sectional temperature distribution of the heavy rail steel bloom at various positions

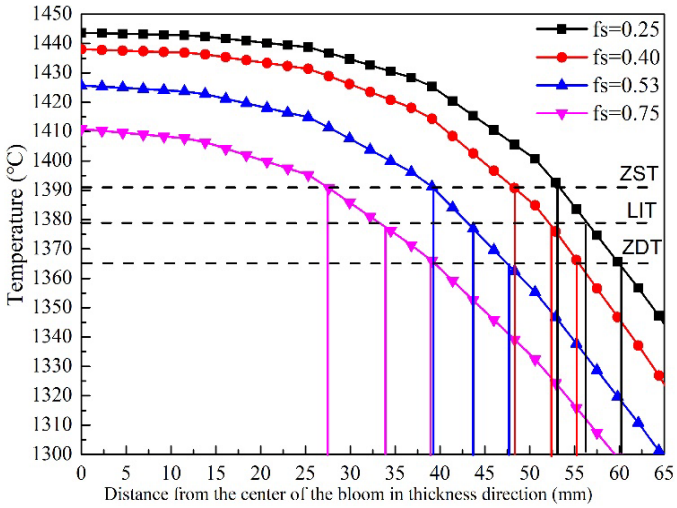

Fig. 7. Temperature distribution in thickness direction of heavy rail steel bloom at various positions

3.2. Influence of reduction parameters on strain of the bloom

Fig. 8 illustrates the strain distribution of PE11 in the cross section of the heavy rail steel casting bloom, where PE11 denotes the plastic strain in the x direction. Subfigures 8(a), 8(b), 8(c), and 8(d) present the PE11 distribution across the bloom cross-section at central solid fractions of 0.25, 0.40, 0.53, and 0.75, respectively. As shown in Fig. 8, when the bloom reduction was 1 mm, the PE11 strain across the cross section was negligible, indicating minimal strain development. However, at a reduction of 3 mm, the PE11 strain increased noticeably, particularly at the four corners of the bloom's cross-section. When the bloom reduction reached 5 mm, the PE11 strain at the four corners of the cross-section increased further. This indicates that the PE11 strain at the corner of the bloom progressively intensified with increasing reduction.

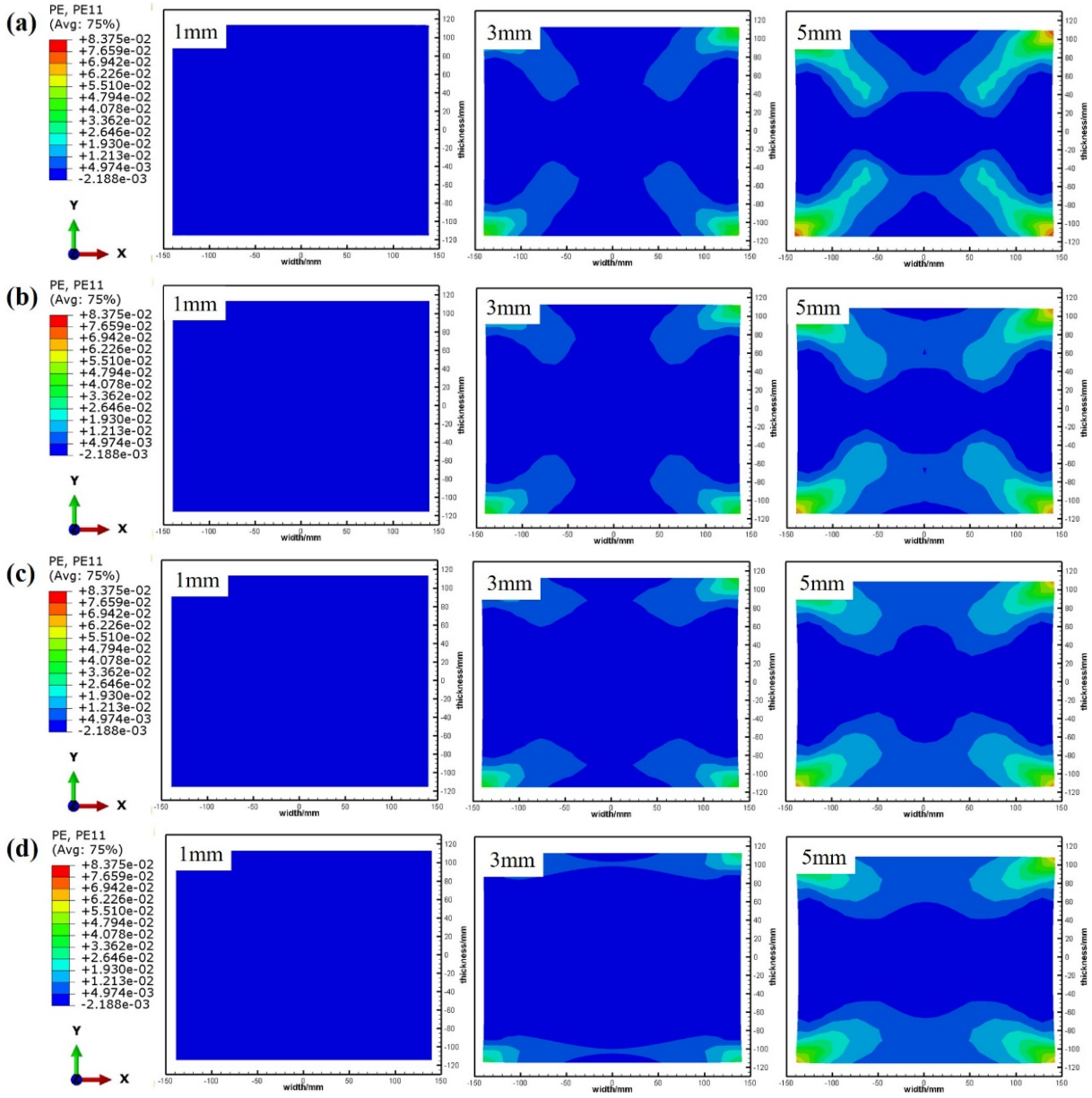

Fig. 8. The strain distribution of PE11 in the cross section of the heavy rail steel casting bloom; (a) 0.25; (b) 0.40; (c) 0.53; (d) 0.75

Fig. 9 illustrates the PE11 strain distribution along the solidification front in the thickness direction of the heavy rail steel bloom under different reduction amounts. The reductions were applied at the position corresponding to a central solid fraction of 0.25. The crack-sensitive zone was located 56.2-60.1 mm from the bloom centre, along the thickness direction. When the bloom was reduced by 1 mm, 3 mm, and 5 mm, the PE11 strain within this zone was 0.00%, 0.28%, and 0.58-0.65%, respectively. The bloom was reduced at the position corresponding to a central solid fraction of 0.40. The crack sensitive zone was located 52.5-55.3 mm from the bloom center along the thickness direction. When the bloom was reduced by 1 mm, 3 mm, and 5 mm, the PE11 strain within this zone was 0.00%, 0.06%~0.07% and 0.58%-0.62%, respectively. The bloom was reduced at the position corresponding to a central solid fraction of 0.53. The crack-sensitive zone was located 43.8-47.8 mm from the bloom centre, along the thickness direction. Under reductions of 1 mm, 3 mm, and 5 mm, the PE11 strain in this zone was 0.00%, 0.00%, and 0.22%-0.23%, respectively. The bloom was reduced at the position corresponding to a central solid fraction of 0.75. The crack-sensitive zone was located 33.9-39.0 mm from the bloom centre, along the thickness direction. When the bloom was reduced by 1 mm, 3 mm, and 5 mm, the PE11 strain within the zone was 0.00%, 0.00%, and 0.07%-0.12%, respectively.

Therefore, the PE11 strain in the crack-sensitive zone increased with greater reduction amounts, while it decreased with increasing central solid fraction. This indicates that when the bloom is reduced at positions with a lower central solid fraction, the PE11 strain at the solidification front is higher, making the bloom more susceptible to internal crack formation. When the bloom was reduced at a position with a higher central solid fraction, the PE11 strain at the solidification front was relatively low, thereby reducing the bloom's susceptibility to internal crack formation. In summary, given that the critical strain for the heavy rail steel grade was 0.40%, no risk of internal crack formation was observed when the reduction per roll was 1 mm and 3 mm. However, at a reduction of 5 mm per roll, internal crack formation became likely when the central solid fraction of the bloom was below 0.40.

3.3. Industrial test of heavy rail steel bloom with reduction

An industrial reduction test was conducted on a 230 mm × 280 mm heavy rail steel bloom. At casting speeds of 0.90 m/min, 0.95 m/min, 1.00 m/min, and 1.05 m/min, the distances between the solidification end point and the meniscus were 17.8 m, 18.8 m, 19.7 m, and 20.5 m, respectively. The distances between rollers 0#~5# and the meniscus were 14.2 m, 15.9 m, 17.1 m, 18.3 m, 19.5 m, and 20.7 m, respectively. The spacing between rollers 0# and 1# was 1.70 m, while the spacing between each of rollers 1#–5# was 1.20 m. The central solid fraction of the bloom under different casting speeds is summarized in TABLE 4, and the corresponding reduction schemes are presented in TABLE 5.

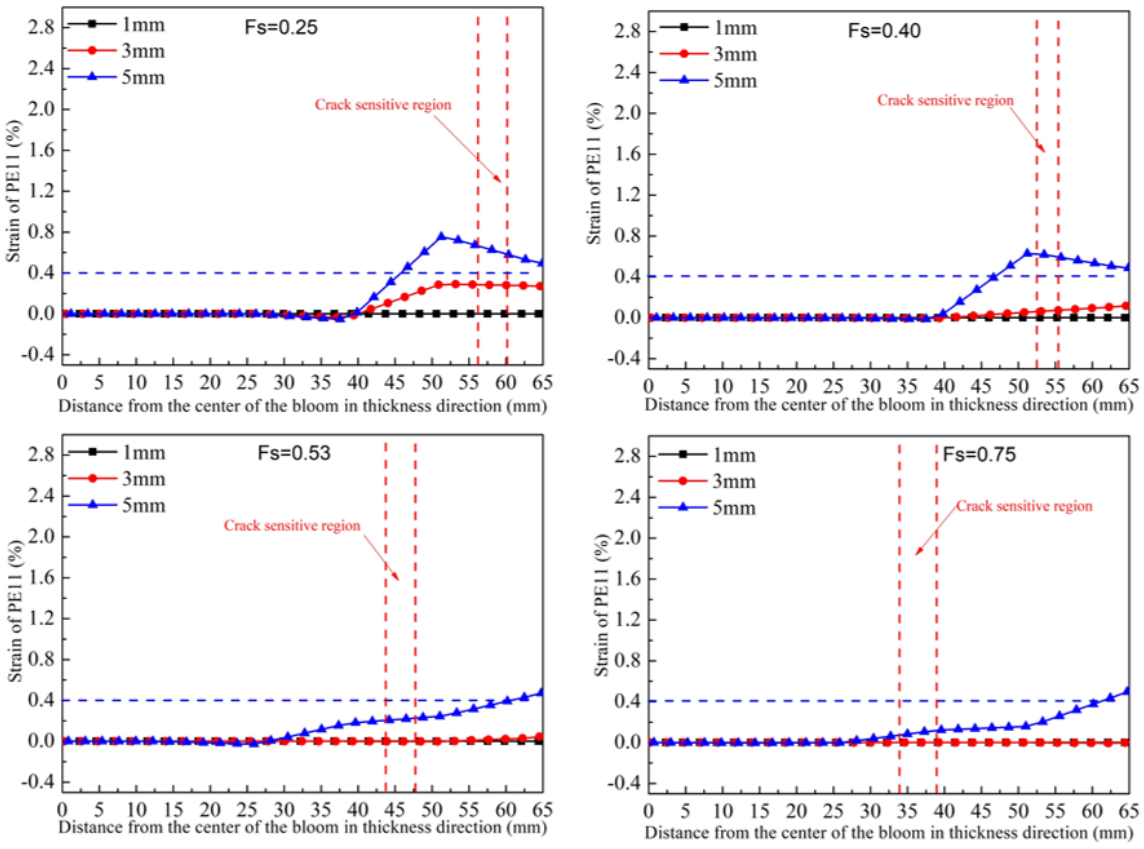

Fig. 9. PE11 at solidification front of the bloom with different reduction amount

TABLE 4

Central solid fraction of 230 mm × 280 mm heavy rail steel

No.	Section /mm²	Casting Speed m/min	Casting End /m	Solid Fraction						
				0#	1#	2#	3#	4#	5#	6#
1	230×280	0.90	17.8	0.33	0.56	0.83	1.00	1.00	1.00	1.00
2	230×280	0.95	18.8	0.25	0.40	0.53	0.75	1.00	1.00	1.00
3	230×280	1.00	19.7	0.20	0.30	0.42	0.62	0.92	1.00	1.00
4	230×280	1.05	20.5	0.16	0.26	0.36	0.50	0.68	1.00	1.00

TABLE 5

Casting parameters of heavy rail steel with 230 mm × 280 mm section

No.	Section mm²	Casting Speed m/min	Amount Reduction/mm						
			0#	1#	2#	3#	4#	5#	6#
Case1	230×280	1.05	3	4	4.5	4.5	0	0	0
Case2	230×280	1.00	3	4	4.5	4.5	0	0	0
Case3	230×280	0.95	0	3	7	3	0	0	0
Case4	230×280	0.90	0	2	3	0	0	0	0

Fig. 10 shows the acid-etched longitudinal section of the 230 mm × 280 mm heavy rail steel bloom. As illustrated, at a casting speed of 1.05 m/min, the applied reduction mode was 3-4-4.5-4.5-0-0-0-0 mm, corresponding to a reduction zone located within the central solid fraction of 0.16-0.50, between reduction rolls 0#–3#. The total reduction applied was 16 mm. Serious reduction-induced internal cracks were observed in the bloom. The cracks exhibited lengths ranging from 10 to 40 mm, with a wide opening degree, and the crack tip was located 49 mm from the inner arc side of the bloom. At a casting speed of 1.00 m/min, the reduction mode of 3-4-4.5-4.5-0-0-0 mm was applied. The reduction zone corresponded to a central solid fraction range of 0.20-0.62, located between reduction rolls 0# and 3#, with a total reduction of 16 mm. Compared

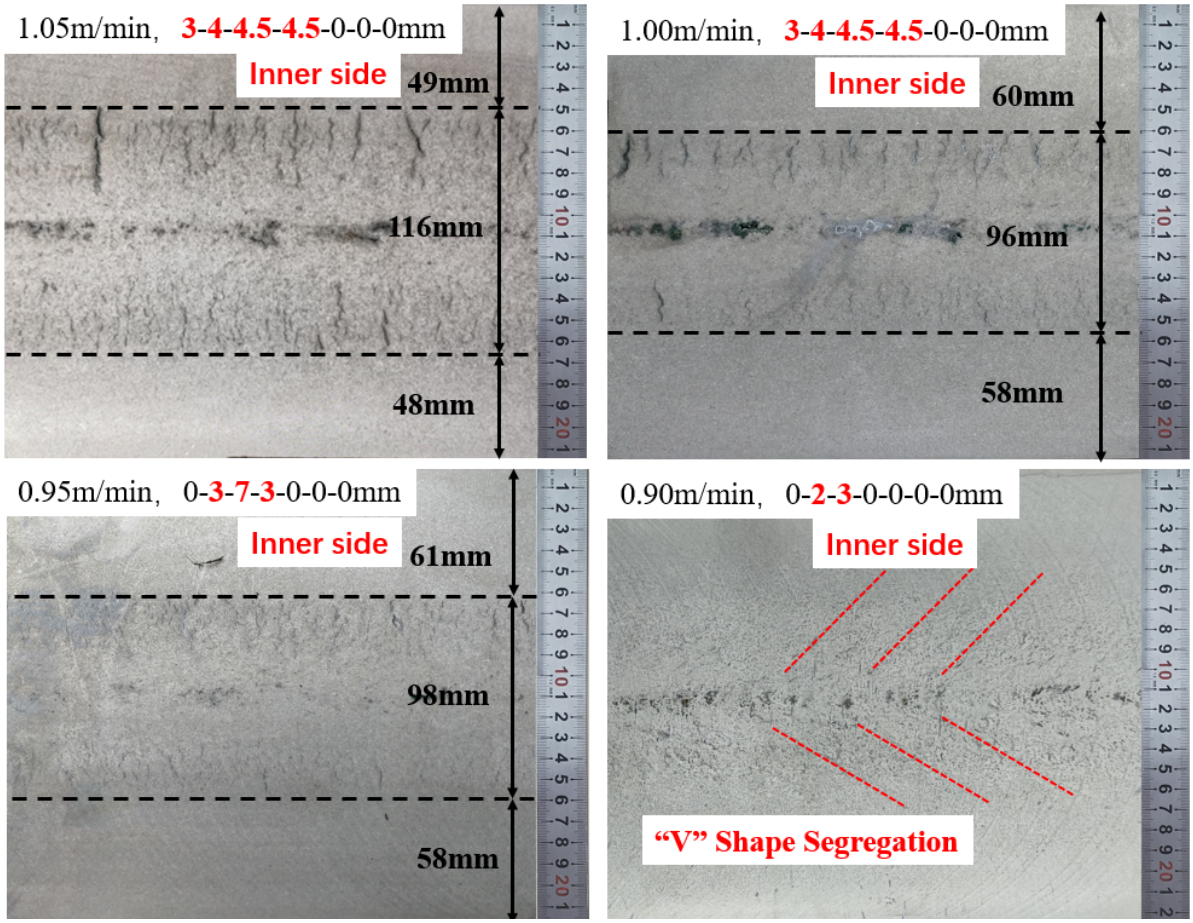

Fig. 10. The acid erosion picture of heavy rail steel sample with 230 mm × 280 mm section

with the Case 1 reduction mode, the severity of internal cracking was reduced, with crack lengths ranging from 10 to 25 mm. The crack opening degree was smaller, and the crack tip was located 60 mm from the inner arc side of the bloom. This indicates that the severity of reduction-induced internal cracks decreases as the reduction zone shifts toward the later stages of solidification. At a casting speed of 0.95 m/min, the reduction mode of 0-3-7-3-0-0-0-0 mm was applied. The reduction zone, spanning rollers 1#–3#, corresponded to a central solid fraction range of 0.40-0.75, with a total reduction of 13 mm. Although the reduction zone was shifted backwards, the 2# roller (at a central solid fraction of 0.53) applied a 7 mm reduction, resulting in the persistence of internal cracks in the bloom. The internal cracks measured 2-5 mm in length, with the crack tip located 61 mm from the inner arc side of the bloom. Although the reduction zone was shifted backwards, the reduction applied by a single roll was excessive, thereby maintaining a high risk of internal crack formation in the bloom. At a casting speed of 0.90 m/min, the reduction mode of 0-2-3-0-0-0-0-0 mm was adopted. The reduction zone, applied at rollers 1#-2#, corresponded to a central solid fraction range of 0.56-0.83, with a total reduction of 5 mm. Under these conditions, no internal cracks were observed in the bloom. Therefore, the occurrence of internal cracks in the bloom was significantly reduced by decreasing the reduction amount and shifting the reduction zone backwards. Based on the above analysis, the crack-sensitive zone of the 230 mm × 280 mm bloom was primarily concentrated in the central solid fractions below 0.42, thereby validating the reliability of the model.

4. Conclusion

This study systematically evaluated the crack risk of 230 mm × 280 mm heavy rail steel blooms through a combination of numerical simulation and industrial validation. The investigation revealed that crack-sensitive zones were located at 56.2-60.1 mm, 52.5-53.3 mm, 43.8-47.8 mm, and 33.9-39.0 mm from the bloom center, corresponding to central solid fractions of 0.25, 0.40, 0.53, and 0.75, respectively. Numerical simulations demonstrated that internal cracks did not occur at per roll reductions of 1 mm and 3 mm. However, when the reduction reached 5 mm and the central solid fraction was below 0.40, the probability of crack formation increased significantly. Industrial trials further confirmed that crack susceptibility was concentrated in regions with central solid fractions below 0.42. Moreover, reducing the per-roll reduction amount or shifting the reduction zone backwards effectively suppressed the risk of crack formation. These findings establish a clear mechanistic link between solidification front characteristics, reduction parameters, and susceptibility to cracking. Beyond prediction, the results offer practical process-control strategies to enhance bloom quality and reliability in heavy rail steel production. Looking forward, further research should address the combined effects of thermal gradients, alloy composition, and dynamic deformation to refine crack-prevention frameworks for industrial practice.

Author Contributions

Writing-original draft, Haitao Ma; Supervision, Yanhui Sun. All authors have read and agreed to the published version of the manuscript.

Funding

This research was funded by the special project of CERI (No. YF241030).

Acknowledgements

The authors would like to express their gratitude to EditSprings (https://www.editsprings.com) for the expert linguistic services provided.

REFERENCES

[1] Y.D. Cen, L. Chen, R. Dong, Q.F. Zhou, Effect of self-tempering on fatigue crack Growth of heavy rail steel. Materials Reports. **35**, 12136-12140 (2021).
DOI: https://doi.org/10.11896/cldb.20050123

[2] H. Sun, L. Li, X. Cheng, W. Qiu, Z. Liu, L. Zeng, Reduction in macrosegregation on 380 mm×490 mm bloom caster equipped combination M+F-EMS by optimising casting speed. Ironmaking & Steelmaking **42**, 439-449 (2015).
DOI: https://doi.org/10.1179/1743281214y.0000000247

[3] H.G. Li, T.M. Chen, L. Chen, Effects of EMS on the dendritic structure and homogeneity of rail steel. Iron Steel Vanadium Titanium **42**, 126-130 (2021).
DOI: https://doi.org/10.7513/j.issn.1004-7638.2021.01.020

[4] H. Wang, J. Wang, Z. Zhang, D.G. Fan, C.H. Jiang, B.B. Zhang, P. Wang, J.Q. Zhang, Soft reduction control investigation of spot segregation in continuous casting bloom for 42CrMoA crankshaft steel. Journal of Iron and Steel Research International **32**, 695-706 (2025). DOI: https://doi.org/10.1007/s42243-024-01295-2

[5] W.G. Hu, C. Ji, M.Y. Zhu, Numerical simulation of continuous casting bloom solidification end reduction process for heavy-haul railway rails. Continuous Casting **04**, 2-6 (2021).
DOI: https://doi.org/10.13228/j.boyuan.issn1005-4006.20210065

[6] J.P. Zhao, L. Liu, J. W. Fan, L. Wang, Study and application of soft reduction technology in continuous casting. Material Reports **30**, 57-61 (2016).
DOI: https://doi.org/10.11896/j.issn.1005-023x.2016.015.009

[7] J. Zeng, W.Q. Chen, Q.X. Wang, G.S. Wang, Improving Inner Quality in Continuous Casting Rectangular Billets: Comparison Between Mechanical Soft Reduction and Final Electromagnetic Stirring. Transactions of the Indian Institute of Metals **69**, 1623-1632 (2016).
DOI: https://doi.org/10.1007/s12666-015-0742-2

[8] B. Wang, J. M. Zhang, C. Xiao, S.X. Wang, W. Song, Formation mechanism of internal cracks in continuous casting slab with soft reduction. Chinese Journal of Engineering **38**, 351-356 (2016).
DOI: https://doi.org/10.13374/j.issn2095-9389.2016.03.008

[9] Z.Y. Liu, X.M. Cao, J.G. Cheng, C.J. Wang, Z. Gao, C.J. Han, H.B. Liu, H.H. An, Analyse and improve intermediate crack in continuous casting slab based on QES. Steelmaking **29**, 14-18 (2019). DOI: CNKI:SUN:LGZZ.0.2013-03-005

[10] G.L. Li, Study on initiation and propagation of intermediate and surface cracks in continuous casting billet. Master Thesis, Northeastern University, Shenyang, January.

[11] G.L. Li, C. Ji, M.Y. Zhu, Prediction of Internal Crack Initiation in Continuously Cast Blooms. Metallurgical and Materials Transactions B **52**, 1164-1178(2021).
DOI: https://doi.org/10.1007/s11663-021-02101-0

[12] P. Wang, L. Chen, Q.W. Tang, W.T. Li, S.X. Li, J.Q. Zhang, Propagation form of internal cracks induced by continuous casting soft reduction and control strategy for internal quality. Journal of Iron and Steel Research International **31**, 622-633 (2024).
DOI: https://doi.org/10.1007/s42243-023-01144-8

[13] X. Song, H. Zhang, H.W. Ni, R.J. Cheng, Q. Fang, C. Liu, Thermo-mechanical Coupled Numerical Simulation of Continuously Casting Heavy Rail Bloom under Soft Reduction Process. Foundry Technology **39**, 1501-1504+1510 (2018).
DOI: https://doi.org/10.16410/j.issn1000-8365.2018.07.030

[14] Y.C. Wang, P. Hu, Research on formation of internal cracks lead by soft reduction in billet continuous casting. Steelmaking **31**, 49-53 (2015). DOI: CNKI:SUN:LGZZ.0.2015-02-012

[15] X.B. Li, H. Ding, Z.Y. Tang, J.C. He, Formation of internal cracks during soft reduction in rectangular bloom continuous casting. International Journal of Minerals, Metallurgy, and Materials **19**, 21-29 (2012).
DOI: https://doi.org/10.1007/s12613-012-0510-9

[16] A. Yamanaka, K. Nakajima, K. Okamura, Critical strain for internal crack formation in continuous casting. Ironmaking and Steelmaking **22**, 508-512 (1995).
DOI: https://doi.org/10.1051/metal/199289070627

[17] S. Kobayashi, Relationships of fraction solid with zero ductility and zero strength temperatures during solidification: Numerical analysis, STEELMAKING, The 114th ISIJ Meeting. 1987

[18] D.G. Enos, J.R. Scully, A critical-strain criterion for hydrogen embrittlement of cold-drawn, ultrafine pearlitic steel. Metallurgical and Materials Transactions A **33**, 1151-1166 (2002).
DOI: https://doi.org/10.1007/s11661-002-0217-z

[19] C. Bernhard, G. Xia, Influence of alloying elements on the thermal contraction of peritectic steels during initial solidification. Ironmaking & Steelmaking **33**, 52-56 (2006).
DOI: https://doi.org/10.1179/174328106X94717

[20] S. Punnose, A. Mukhopadhyay, R. Sarkar, Z. Alam, D. Das, V. Kumar, Determination of critical strain for rapid crack growth during tensile deformation in aluminide coated near-α titanium alloy using infrared thermography. Materials Science & Engineering A **576**, 217-221 (2013).
DOI: https://doi.org/10.1016/j.msea.2013.03.089

[21] J.K. Brimacombe, K. Sorimachi, Crack formation in the continuous casting of steel. Metallurgical Transactions B **08**, 489-505 (1977). DOI: https://doi.org/10.1007/bf02696937

[22] H. Hiebler. Inner crack formation in continuous casting of steel:Stress or Strain Criterion. 1994.